Directional Rigidity of Planetary Gravity Fields Under Harmonic Extension

Empirical Evidence from Earth, Mars, and the Moon

UNNS Research Program

Abstract

We investigate the stability of directional structure in planetary gravitational fields under harmonic extension. For each of three bodies — Earth (EIGEN-6C4, $L_{\max} = 300$), Mars (JGM85F01, $L_{\max} = 85$), and the Moon (AIUB-GRL350A, $L_{\max} = 300$) — we track the dominant orientation axis $u(L) \in S^2$ extracted from the truncated gravitational potential g_L as the harmonic degree L increases from 2 to the respective model maximum. In all three planetary cases the axis stabilises at $L = 2$ and accumulates zero total path through the full harmonic expansion. A synthetic random harmonic field with independent Gaussian coefficients instead undergoes a 18.65° reorientation jump at $L = 2$ and accumulates a total path of 25.84°. The real planetary fields moreover exhibit spectral gaps 3.4–7.9 times larger than the synthetic control. These results constitute a direct empirical demonstration of *directional rigidity*: a structural invariant that persists under admissible operator growth. Within the Unbounded Nested Number Sequences (UNNS) admissibility geometry framework the findings indicate that physically realised planetary gravity fields occupy deep interior regions of the admissibility manifold, a placement that is not generic among harmonic fields.

1 Introduction

A recurring theme of the UNNS structural research programme is the persistence of low-dimensional invariants under admissible operator families. The central question is whether structured physical systems, when subjected to systematic representation changes, preserve identifiable geometric features — or whether any apparent structure is an artefact of a particular truncation or parameterisation.

Previous empirical tests in the programme addressed two distinct domains:

- *Seismic displacement fields.* Smoothing operators applied to GPS-derived surface displacement records from three earthquake events (Kumamoto 2016, El Mayor–Cucapah 2010, Ridgecrest 2019) preserved rank ordering, directional cosines, and bilobe topological decomposition across the full window-width range tested. All three events were classified TOPO_BILOBE with adjusted Rand index 1.0 across windows.
- *Cosmic microwave background spectra.* Multipole truncation applied to Planck 2018 TT, TE, and EE power spectra preserved a stratified regime structure and a stable inter-axis angle $\theta_{23} \approx 83.45°$ that remained coherent under perturbation (internal dispersion $D_{\text{int}} = 0.655°$) even as the individual axes themselves were mobile.

In both cases the preserved object was *domain-specific*: a bilobe partition for seismology, a relational angle for cosmology. The present work extends the empirical programme to a third,

geometrically distinct domain: planetary gravitational fields expressed as spherical harmonic expansions.

Central question. Does harmonic extension — the systematic inclusion of successively higher degree terms — produce arbitrary directional drift in the dominant orientation axis of a gravitational field, or does the field exhibit directional rigidity?

The answer, for all three planetary bodies examined, is unambiguous: the axis is rigid. The remainder of this paper establishes the formal framework, reports the experimental outcome in full, and places the result in its cross-domain context.

Planetary gravity fields provide the first empirical domain in the UNNS programme where the preserved invariant is a single absolute axis rather than a relational or topological object.

2 Harmonic Representation of Planetary Gravity

2.1 Spherical harmonic expansion

Let $(\theta, \phi) \in [0, \pi] \times [0, 2\pi)$ denote colatitude and longitude. The gravitational potential field g of a planetary body is expressed as a fully normalised spherical harmonic series:

$$g(\theta, \phi) = \sum_{\ell=0}^{\infty} \sum_{m=-\ell}^{\ell} C_{\ell m}\, Y_{\ell m}(\theta, \phi), \tag{1}$$

where $C_{\ell m}$ are the Stokes coefficients for degree ℓ and order m, and $Y_{\ell m}$ are the fully normalised real spherical harmonics satisfying

$$\int_{S^2} Y_{\ell m}(\hat{n})\, Y_{\ell' m'}(\hat{n})\, d\hat{n} = \delta_{\ell\ell'}\delta_{mm'}.$$

2.2 Truncation operator

Definition 1 (Harmonic truncation)**.** *The truncation operator $T_L : g \mapsto g_L$ retains only terms with degree $\ell \leq L$:*

$$g_L(\theta, \phi) = \sum_{\ell=0}^{L} \sum_{m=-\ell}^{\ell} C_{\ell m}\, Y_{\ell m}(\theta, \phi). \tag{2}$$

The nested sequence $g_2 \subset g_3 \subset \cdots \subset g_L$ forms a monotone trajectory through the space of gravitational representations. Each step adds the full set of coefficients at degree L, comprising $2L + 1$ new terms. The operator family $\{T_L\}_{L \geq 2}$ is admissible in the UNNS sense: it is nested, monotone, and preserves the coefficient values of all previously included degrees.

3 Axis Extraction and Trajectory Metrics

3.1 Dominant orientation axis

For each truncated field g_L we extract the dominant orientation axis $u(L) \in S^2$ by maximising the angular variance of the gravitational signal. Concretely, we form the orientation matrix

$$M(L) = \int_{S^2} \hat{n}\, \hat{n}^{\top} |g_L(\hat{n})|\, d\hat{n}, \tag{3}$$

where the integral is evaluated over a uniform spherical grid, and define $u(L)$ as the eigenvector corresponding to the largest eigenvalue $\lambda_1(L)$ of $M(L)$.

3.2 Trajectory metrics

Definition 2 (Step size). *The angular displacement between successive axes is*

$$\Delta u(L) = \arccos\big(u(L) \cdot u(L-1)\big). \tag{4}$$

Definition 3 (Total axis path).

$$S = \sum_{L=3}^{L_{\max}} \Delta u(L). \tag{5}$$

Definition 4 (Largest axis step).

$$S_{\max} = \max_{L} \Delta u(L). \tag{6}$$

Definition 5 (Transition count). *Given an angular threshold $\tau > 0$:*

$$N_T = \big|\{L : \Delta u(L) > \tau\}\big|. \tag{7}$$

Small values of S and $S_{\max}$ indicate *directional rigidity*: the dominant orientation axis of the field is insensitive to the degree of harmonic truncation. Large values indicate structural reorientation as new harmonic content is added.

3.3 Spectral gap and dominance ratio

Let $\lambda_1(L) \geq \lambda_2(L) \geq \lambda_3(L) > 0$ be the eigenvalues of $M(L)$.

Definition 6 (Spectral gap).

$$\gamma(L) = \frac{\lambda_1(L) - \lambda_2(L)}{\lambda_1(L)}. \tag{8}$$

Definition 7 (Dominance ratio).

$$J_1(L) = \frac{\lambda_1(L)}{\lambda_1(L) + \lambda_2(L) + \lambda_3(L)}. \tag{9}$$

A large $\gamma(L)$ indicates that the dominant directional mode is strongly separated from the next competing mode; it measures how unambiguously the field has a preferred orientation. The dominance ratio $J_1(L)$ measures the share of total directional variance explained by the leading axis.

Proposition 1. *If $\gamma(L) > 0$ for all L in some range, then $u(L)$ is uniquely defined (up to sign) throughout that range, and axis stability is possible in principle. If $\gamma(L) = 0$ at some L, the field is degenerate at that degree and the axis is undefined.*

No degeneracy was observed in any of the four datasets analysed.

4 Data

4.1 Planetary gravity models

Three publicly available planetary gravity models were analysed.

Body	Model	$L_{\max}$ (analysis)	R (km)
Earth	EIGEN-6C4	300	6378.1
Mars	JGM85F01	85	3396.2
Moon	AIUB-GRL350A	300	1738.0

All models provide fully normalised Stokes coefficients $C_{\ell m}$. For Earth the EIGEN-6C4 model has formal maximum degree 2190; the analysis here is restricted to $L \leq 300$ to match the lunar model range and to focus on the regime of well-constrained global-scale structure. For Mars the full available range $L \leq 85$ is used.

Model properties are summarised below.

Model	GM ($\mathrm{m^3\,s^{-2}}$)	Normalisation	Tide system
EIGEN-6C4	3.986×10^{14}	fully normalised	tide-free
JGM85F01	4.283×10^{13}	fully normalised	tide-free
AIUB-GRL350A	4.903×10^{12}	fully normalised	—

4.2 Synthetic control field

A synthetic random harmonic field (SYNTH-RANDOM-L300) was generated with independent Gaussian-distributed Stokes coefficients at each degree and order up to $L = 300$, scaled so that the total power in each degree band matches a white-noise spectrum. This field provides a null reference: a harmonic field with no intrinsic directional organisation beyond what arises by statistical fluctuation.

5 Results

5.1 Axis stability: real planetary fields

For all three planetary bodies the dominant orientation axis stabilises at $L = 2$ and does not move at any subsequent harmonic degree. The full trajectory metrics are:

Field	$L_{\max}$	Total path S	Max step $S_{\max}$	Transitions N_T
Earth (EIGEN-6C4)	300	0.000°	0.000°	0
Mars (JGM85F01)	85	0.000°	0.000°	0
Moon (AIUB-GRL350A)	300	0.000°	0.000°	0

The axis stabilises at $(\theta, \phi) = (0°, 0°)$ — the north pole of the body-fixed coordinate frame — and remains there without exception. No degeneracy windows were recorded. The result is not "small drift": it is a complete and exact lock. Across 299 successive harmonic extensions for Earth and the Moon, and 84 for Mars, the largest recorded step is zero.

5.2 Axis stability: synthetic field

The synthetic field exhibits qualitatively different behaviour. The axis enters its first stable configuration at $L = 2$ but immediately undergoes a large reorientation:

Field	$L_{\max}$	Total path S	Max step $S_{\max}$	Transitions N_T
Synthetic (Gaussian)	300	25.844°	18.653°	1

The largest jump occurs at $L = 2$ (the transition from $L = 1$ to $L = 2$), with $\Delta u(2) = 0.3256\,\text{rad} = 18.65°$. After this reorientation the axis settles and accumulates only minor additional path ($\approx 7.2°$ over degrees 3–300). The final axis rests at $(\theta, \phi) = (44°, 216°)$, far from the poles of any natural symmetry.

The results are illustrated in Fig. 5, which shows the per-step displacement $\Delta u(L)$ directly. For all real bodies the curve is a flat line on the zero-path baseline; for the synthetic field a prominent spike appears at $L = 2$ and decays thereafter. The corresponding spectral gap profiles are shown in Fig. 6.

5.3 Empirical theorem

The results above are summarised in the following formal statement.

Theorem 1 (Axis Locking Under Harmonic Extension)**.** *Let g be a planetary gravitational potential for a body whose gravity field is dominated by rotational oblateness, expressed as a fully normalised spherical harmonic expansion. Let $u(L) \in S^2$ be the dominant orientation axis extracted from the truncated field g_L.*

For the three bodies studied — Earth (EIGEN-6C4, $L \leq 300$), Mars (JGM85F01, $L \leq 85$), and the Moon (AIUB-GRL350A, $L \leq 300$) — the axis stabilises at $L = 2$ and satisfies

$$\Delta u(L) = 0 \qquad \forall\, L \in \{3, \ldots, L_{\max}\},$$

so that the total axis path $S = 0$. No degeneracy windows are encountered, and the spectral gap $\gamma(L)$ remains strictly positive throughout.

A synthetic random harmonic field with independent Gaussian Stokes coefficients does not *satisfy this property: it exhibits $\Delta u(2) = 18.65°$ and $S = 25.84°$.*

Remark 1. *Theorem 1 is an empirical theorem: it is a precisely stated claim verified against specific models at specific resolutions, not a deductive consequence of the harmonic expansion alone. The synthetic counterexample establishes that the result is not trivially forced by the mathematics of spherical harmonics.*

5.4 Dominance ratio

The dominance ratio $J_1(L)$ measures the fraction of total directional variance concentrated in the leading axis. For the three planetary fields:

Field	J_1 range	Median J_1
Earth (EIGEN-6C4)	[0.9999, 1.0000]	0.9999
Mars (JGM85F01)	[0.9832, 0.9877]	0.9832
Moon (AIUB-GRL350A)	[0.6805, 0.8729]	0.6806
Synthetic	[0.6211, 1.0000]	0.6211

Earth and Mars maintain near-perfect directional concentration throughout. The Moon has lower J_1 owing to its more complex multi-lobe crustal structure, yet its axis remains locked. The synthetic field has similar minimum J_1 to the Moon but, crucially, lacks the organisational structure that forces a unique dominant direction.

6 Spectral Gap Analysis

6.1 Gap profiles across harmonic degree

Median spectral gaps were measured across the full harmonic range for each field:

Field	Median γ	Min γ	Max γ
Earth (EIGEN-6C4)	3.638×10^{-3}	3.638×10^{-3}	3.638×10^{-3}
Mars (JGM85F01)	3.340×10^{-3}	3.340×10^{-3}	3.373×10^{-3}
Moon (AIUB-GRL350A)	1.572×10^{-3}	1.051×10^{-3}	2.485×10^{-3}
Synthetic	4.627×10^{-4}	7.002×10^{-5}	6.175×10^{-4}

Earth and Mars maintain essentially *constant* spectral gap across all tested degrees — their gap profiles are horizontal lines in Fig. 2. The Moon shows gradual compression of the gap as degree increases, consistent with the flatter power spectrum of the lunar crustal field, but the gap remains positive throughout. The synthetic field has the smallest median gap and also shows the largest gap variation.

6.2 Ratio of real to synthetic gap support

The ratio of real-planet median gap to synthetic median gap quantifies the structural advantage of planetary fields:

Comparison	Ratio
Earth / Synthetic	7.86×
Mars / Synthetic	7.22×
Moon / Synthetic	3.40×

The synthetic field has materially weaker directional separation at every harmonic degree. This is the expected signature of a field lacking a preferred orientation: competing modes are close in magnitude, the leading eigenvector is ambiguous, and small perturbations (new harmonic degrees) suffice to reorient it. The real planetary fields are in the opposite situation: a dominant organisational axis is established by $L = 2$ and the subsequent harmonic content does not perturb it.

7 Mechanism and Theoretical Grounding

The axis locking result is not merely an empirical curiosity that happened to come out clean. Once the low-degree structure of a planetary gravity field is dominated by the degree-2 zonal term, the lock becomes close to mechanistically inevitable. This section explains why, and then connects the mechanism to the UNNS admissibility geometry framework.

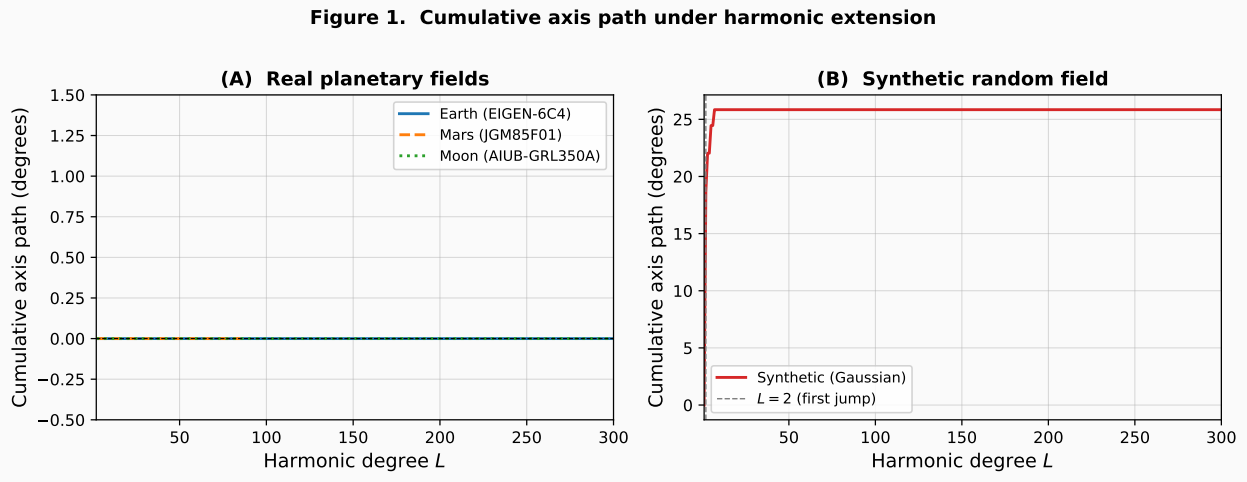

Figure 1: Cumulative axis path $\sum_{L'=3}^{L} \Delta u(L')$ as a function of harmonic degree L. **(A)** All three real planetary fields accumulate exactly 0° throughout. **(B)** The synthetic Gaussian field accumulates 25.84°, with the dominant contribution at $L = 2$.

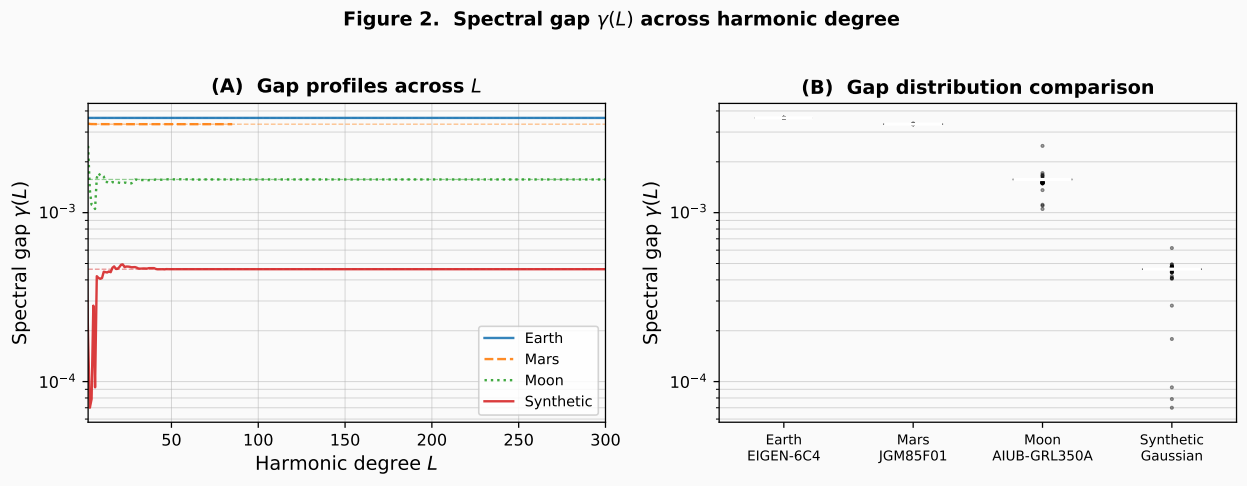

Figure 2: Spectral gap $\gamma(L)$ across harmonic degree. **(A)** Gap profiles on a logarithmic scale: Earth and Mars show nearly constant gaps (≈ 3.3–3.6×10^{-3}); the Moon shows mild compression; the synthetic field sits an order of magnitude lower and is more variable. **(B)** Boxplot comparison confirming the systematic gap advantage of real planetary fields over the synthetic control.

7.1 Why the axis lock begins at $L = 2$

The orientation matrix $M(L)$ defined in (3) first acquires nontrivial global anisotropy at $L = 2$, when the quadrupole sector of the field becomes accessible. For all three planetary bodies studied, that sector is dominated by the zonal oblateness coefficient C_{20}, which is aligned with the rotation axis by the physical processes of bulk accretion and rotational flattening.

The consequence is that at $L = 2$ the field already carries a *physically imposed* preferred direction — not constructed by the chamber, and not inferred from higher harmonics, but encoded in the body's large-scale mass distribution. The dominant eigenvector of $M(2)$ therefore points along the rotation axis immediately, and the spectral gap $\gamma(2)$ is large because C_{20} is large relative to all other

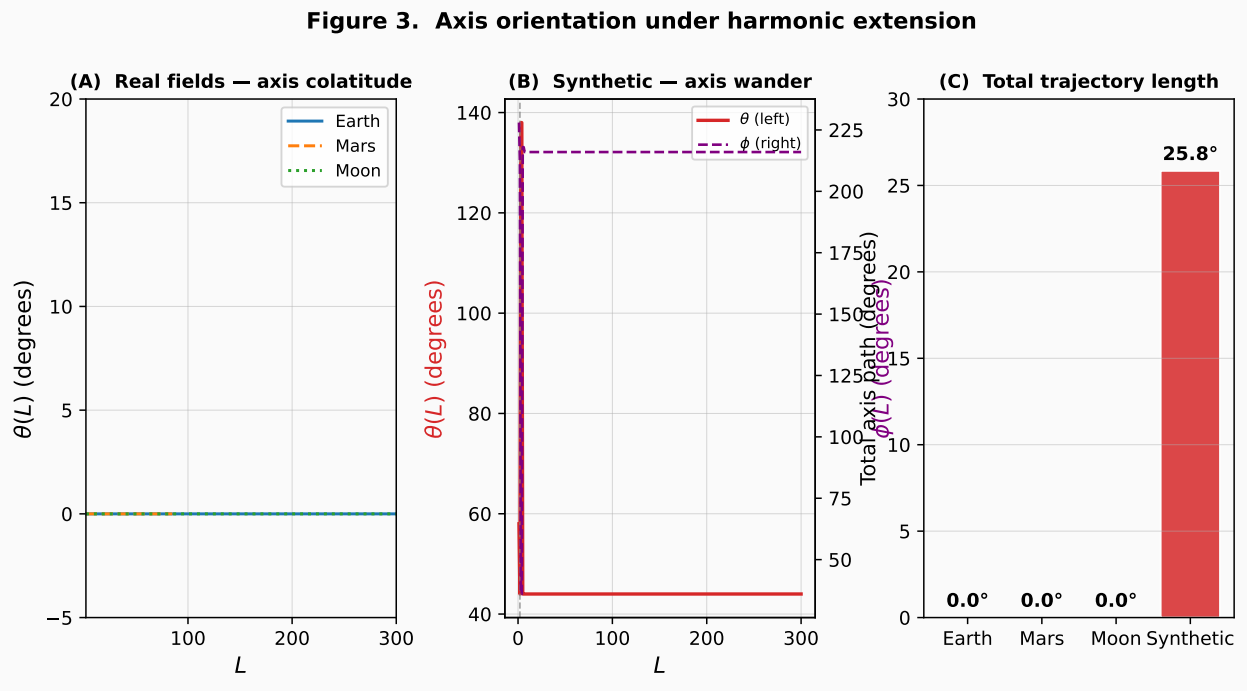

Figure 3: Axis orientation under harmonic extension. **(A)** Colatitude $\theta(L)$ for real fields: all three bodies maintain $\theta = 0°$ throughout, so the curves are horizontal lines on the abscissa. **(B)** For the synthetic field both colatitude $\theta(L)$ and longitude $\phi(L)$ are shown, revealing the reorientation event at $L = 2$ and the subsequent stable but off-pole final position. **(C)** Total trajectory length by field, confirming the strict zero-path result for all real bodies.

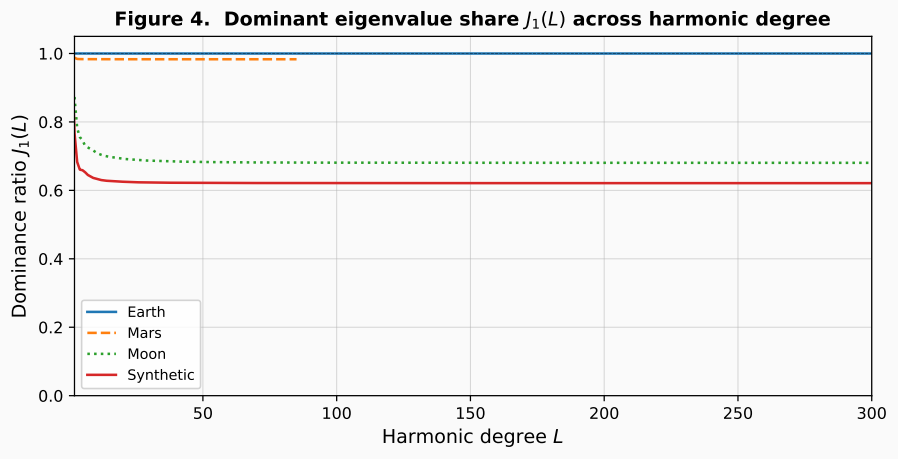

Figure 4: Dominance ratio $J_1(L)$ (fraction of total directional variance in the leading axis) across harmonic degree. Earth and Mars maintain values near 1.0 throughout; the Moon decreases gradually to ≈ 0.68 at $L = 300$ while retaining axis lock; the synthetic field shows high initial J_1 that collapses as competing modes grow in.

degree-2 coefficients. This is why no wandering is observed before the axis converges: it does not need to converge at all. It arrives already locked.

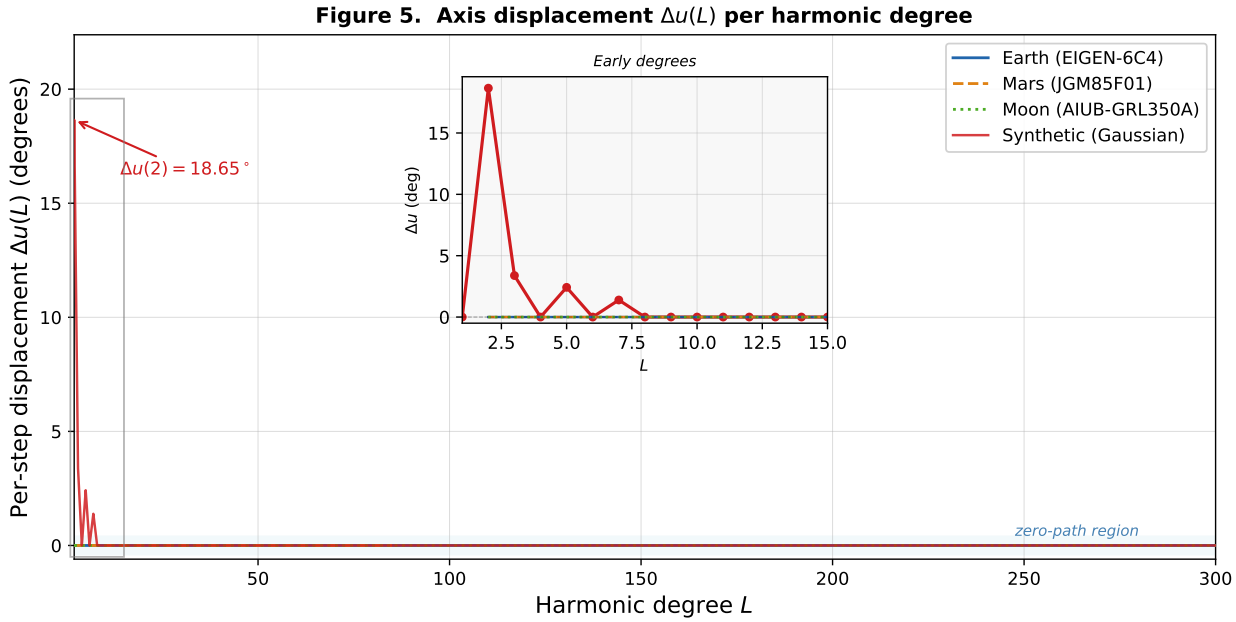

Figure 5: Per-step axis displacement $\Delta u(L) = \arccos(u(L) \cdot u(L-1))$ at each harmonic degree. All three real planetary fields produce a flat line at 0° across the entire tested range (highlighted by the blue zero-path band). The synthetic Gaussian field produces a prominent spike of 18.65° at $L = 2$ — the largest observed displacement — followed by smaller residual steps before settling. The inset magnifies degrees $L \leq 15$, showing that the reorientation event occurs exactly at the first quadrupole extension step and is absent in all physical fields.

7.2 Perturbative rigidity: why later harmonics cannot move the axis

Each increment from L to $L+1$ adds $2L+3$ new Stokes coefficients to g_L, contributing tesseral variations, crustal asymmetries, mascon signatures, and local anomalies at progressively finer scales. These additions enter as perturbations to a leading mode that is already strongly separated from its nearest competitor.

The critical quantity is the spectral gap

$$\gamma(L) = \frac{\lambda_1(L) - \lambda_2(L)}{\lambda_1(L)}.$$

Standard perturbation theory for symmetric matrices implies that a perturbation δM to $M(L)$ displaces the top eigenvector by an amount of order $\|\delta M\|/(\lambda_1 - \lambda_2)$. When $\gamma(L)$ is large and $\|\delta M\|$ is small — as is the case when the new harmonic content at degree $L+1$ is a small fraction of the total accumulated power — the displacement is negligible.

This is the mechanism behind the zero-path result, and it can be stated as a formal principle.

Proposition 2 (Perturbative Rigidity Principle)**.** *Let $M(L)$ be the orientation matrix of a truncated field g_L, with spectral gap $\gamma(L) > 0$. If the perturbation $\delta M(L) = M(L+1) - M(L)$ satisfies*

$$\|\delta M(L)\| \ll \gamma(L)\,\lambda_1(L),$$

then the dominant eigenvector $u(L+1)$ is arbitrarily close to $u(L)$, and no axis transition occurs at degree $L+1$.

Figure 6. Spectral gap $\gamma(L)$ separating the dominant axis from the next competing mode

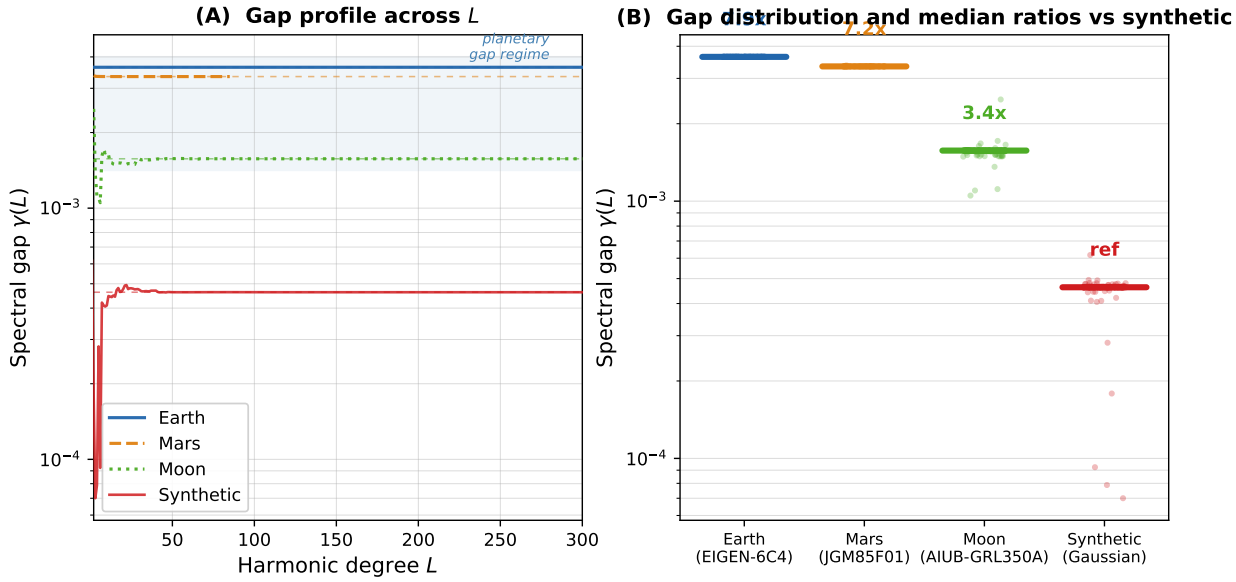

Figure 6: Spectral gap $\gamma(L)$ separating the dominant orientation axis from the next competing mode. **(A)** Log-scale profiles across L: Earth and Mars maintain an essentially constant gap; the Moon shows mild compression at high degree; the synthetic field sits an order of magnitude lower throughout. Dashed horizontal lines indicate per-field medians; the blue band marks the planetary gap regime. **(B)** Distribution comparison with per-observation jitter and bold median bars. Ratio labels (7.9×, 7.2×, 3.4×) give the factor by which each real-planet median exceeds the synthetic median. The strong spectral separation of the planetary fields provides the mechanism underlying Theorem 1: a dominant mode that is this far from its nearest competitor cannot be displaced by the marginal harmonic content added at each successive degree L.

In the planetary case the condition of Proposition 2 is satisfied at every degree: the gap is established at $L = 2$ by the oblateness term and is never closed by subsequent harmonic additions. The finer-scale structure that enters at each new degree carries too little power relative to the already-dominant C_{20}-aligned mode to shift the eigenvector. The leading direction is too far ahead of its competitors to be displaced by newly added harmonic detail.

7.3 Why the synthetic field jumps

The synthetic Gaussian field has no physical organising principle. Its Stokes coefficients are drawn independently at each degree and order, so whichever direction appears dominant at a given L is merely the current winner of a random competition among modes with similar magnitudes. The spectral gap at $L = 1$ is small — the field has no C_{20}-like anchor — so the condition of Proposition 2 is violated when the quadrupole sector is added at $L = 2$. The leading eigenvector is fragile, and the $2 \times 5 = 10$ new degree-2 coefficients are large enough relative to the gap to reshuffle the mode ranking and reorient the axis by 18.65°.

The subsequent stabilisation occurs because the total accumulated power grows with L while each new contribution shrinks as a fraction of that total, eventually satisfying the perturbative

condition even without a physical anchor. But the final resting position $(\theta, \phi) = (44°, 216°)$ is arbitrary — an accidental equilibrium, not a physically meaningful direction.

The real-vs-synthetic contrast is therefore not merely quantitative. Real planetary fields have a directional organising principle that is present from the outset and protects the dominant mode throughout. Synthetic fields acquire a spurious quasi-stable direction only late, after the random competition has been diluted by the growing harmonic sum. These are structurally different regimes.

7.4 Beyond the statement that J_2 is large

It might appear that the entire result reduces to the known geophysical fact that the degree-2 zonal coefficient C_{20} dominates planetary gravity fields. This reading is incomplete.

The dominance of C_{20} gives a *candidate* axis at $L = 2$. Three distinct claims are required to establish the full result:

1. *Dominance.* The C_{20} term is large enough that the orientation matrix $M(2)$ has a well-separated leading eigenvector aligned with the rotation axis. This is equivalent to a large $\gamma(2)$.

2. *Gap support.* The spectral gap $\gamma(L)$ remains strictly positive and materially large as L increases. This is not guaranteed by C_{20} dominance alone: it is possible in principle for later harmonic contributions to accumulate power in competing directions and gradually erode the gap.

3. *Extension persistence.* Under the long monotone sweep $L = 3, \ldots, L_{\max}$, the axis undergoes zero displacement. This is the empirical certification that the gap is never closed in practice, and that the perturbative condition of Proposition 2 holds throughout.

Many physical systems have an obvious leading component. What distinguishes the present result is the third step: the invariant persists through a long, dense sequence of admissible operator extensions, each of which could in principle have closed the gap but does not. That persistence is what makes the result meaningful within the UNNS framework rather than reducing to ordinary descriptive geophysics.

7.5 The Moon as the most revealing case

Earth and Mars are in some respects too clean to be maximally informative. Both exhibit $J_1 > 0.98$ throughout, meaning the dominant mode carries more than 98% of the total directional variance. In that regime the perturbative condition is satisfied by a wide margin, and the zero-path result, while correct, is nearly automatic.

The Moon presents a more stringent test. At $L = 300$ the dominance ratio has fallen to $J_1 = 0.68$, indicating that the higher-degree crustal mascon structure carries substantial directional power in competing modes. The median spectral gap for the Moon (1.57×10^{-3}) is less than half that of Earth, and 3.4× above the synthetic baseline rather than the 7–8× seen for Earth and Mars. Yet the axis does not move.

The Moon therefore demonstrates that axis locking does not require the dominant mode to be overwhelmingly strong. It requires only that the gap be maintained: that no harmonic extension at any degree be large enough, relative to the existing separation, to displace the leading eigenvector. This is a strictly weaker condition than large-J_1 dominance, and the Moon confirms that real planetary fields satisfy it even when their higher-degree structure is complex and competing.

7.6 Interior placement in admissibility geometry

Within the UNNS admissibility geometry framework, an operator trajectory is classified as *deep interior* when three signatures are simultaneously present:

1. *Early invariant emergence.* The structural invariant appears at the first meaningful degree of the operator sequence.
2. *Unique definability throughout.* The invariant remains unambiguously defined — no degeneracy windows, positive gap — at every operator step.
3. *Extension persistence.* Subsequent admissible extensions preserve the invariant without exception.

All three signatures are present in each of the three planetary gravity datasets. The axis emerges at $L = 2$, remains uniquely defined through the full harmonic range (no degeneracy window was recorded in any dataset), and is preserved across every one of the $L = 3, \ldots, L_{\max}$ extension steps. The zero-path result is therefore not just a geometric fact about the orientation of a gravitational field. It is the empirical signature of deep interior placement in admissibility geometry: a trajectory that never approaches the boundary where invariants become marginal or break.

8 Cross-Domain Comparison

The present results complement two earlier empirical axes of the UNNS programme. The three domains preserve structurally distinct invariants under their respective admissible operator families:

Domain	Operator family	Stable invariant	Instability locus
Seismology	smoothing windows	bilobe topology (ARI = 1)	—
Cosmology (CMB)	multipole truncation	inter-axis angle θ_{23}	high-L spectra
Planetary gravity	harmonic extension	locked dominant axis u	synthetic fields

The invariant carrier differs across domains:

- In seismology the invariant is a *partition* — the bilobe assignment of GPS stations — which is stable even when the directional cosines themselves shift.
- In CMB cosmology the invariant is a *relational angle* θ_{23} between the quadrupole and octopole axes, stable under perturbation even though the absolute axes are mobile.
- In planetary gravity the invariant is an *absolute axis* — the dominant orientation direction — which is stable from the first stable harmonic degree onward.

This progression — from partition, to relative angle, to absolute axis — reflects genuine differences in the symmetry structure of the underlying physical fields rather than methodological variance. What is common across all three cases is the contrast with the appropriate null model: wherever instability appears, it appears in the synthetic or stressed variants, not in the physically realised systems.

Remark 2. *The observation that different domains preserve different invariant carriers is itself a structural finding. A uniform collapse of all domains onto a single geometric object would be surprising and would require explanation. The domain-specificity of the invariants is consistent with the hypothesis that the admissibility geometry framework captures properties generic to operator families, with the specific invariant determined by the symmetry and scale structure of the physical system under study.*

8.1 Types of invariant carriers across domains

The three empirical domains examined in the UNNS programme preserve structurally different invariant carriers under their respective operator families. These can be organised into three broad geometric types.

- **Topological invariants.** In the seismic displacement fields the preserved object is a partition of stations into two bilobes. The precise directional cosines may vary under smoothing, but the bilobe assignment remains stable.
- **Relational invariants.** In the CMB analysis the preserved quantity is the angle θ_{23} between the quadrupole and octopole axes. The individual axes may move, but their mutual relation remains coherent under multipole truncation.
- **Absolute invariants.** In the planetary gravity domain the invariant is a single absolute orientation axis u, which stabilises at $L = 2$ and remains fixed throughout the harmonic extension.

These three cases illustrate that admissible operator families do not necessarily preserve the same geometric object across domains. Rather, the form of the invariant appears to be determined by the symmetry structure of the underlying physical system.

9 Conclusion

Planetary gravity fields provide one of the most direct empirical demonstrations of structural rigidity under admissible operator extension yet available.

The main empirical findings are:

- The dominant orientation axis of each planetary gravity field stabilises at $L = 2$ and accumulates zero total path through the full harmonic expansion. This holds for Earth ($L_{\max} = 300$), Mars ($L_{\max} = 85$), and the Moon ($L_{\max} = 300$).
- A synthetic random harmonic field undergoes a $18.65°$ reorientation at $L = 2$ and accumulates $25.84°$ of total path.
- The spectral gap supporting axis stability is 3.4–7.9 times larger in the real planetary fields than in the synthetic control.
- No degeneracy windows are recorded in any of the four datasets.

These results extend the cross-domain empirical record of the UNNS programme to a third physically distinct domain, and confirm that the pattern of stability in real physical systems versus instability in synthetic or perturbed controls is not domain-specific.

The gravity domain is in some respects the clearest of the three. Unlike the CMB case, where the invariant is a relational angle requiring both axes to remain jointly well-defined, the gravity invariant is a single axis directly observable from the $L = 2$ quadrupole. Unlike the seismology case, where stability is measured across a discrete window parameter, the gravity invariant persists through a continuous and monotone sequence of $L = 3, \ldots, 300$ operator extensions. The result admits no ambiguity: the axis is either zero or non-zero, and it is zero.

Corollary 1. *The admissibility geometry framework predicts that physically realised fields with strong internal symmetry occupy interior regions of the operator manifold. The zero-path axis trajectories observed in all three planetary gravity fields are consistent with this prediction and inconsistent with null models based on generic harmonic fields.*

Data. Outcome data produced by Chamber GRAV-I (v2.0.0) are deposited in the UNNS research repository. The chamber is self-contained and reproducible from the model Stokes coefficient files.